Inorganic Chemistry

Article

pubs.acs.org/IC

A Family of Lanthanide-Based Coordination Polymers with Boronic Acid as Ligand

Xiao Fan,[†] Stéphane Freslon,[†] Carole Daiguebonne,*[,†] Laurent Le Pollès,[‡] Guillaume Calvez,[†] Kevin Bernot,[†] Xiaohui Yi,[†] Gang Huang,[†] and Olivier Guillou*[,†]

[†]INSA, UMR 6226 and [‡]ENSCR, UMR 6226, Institut des Sciences Chimiques de Rennes, F-35708 Rennes, France

Supporting Information

ABSTRACT: Reactions in water between the sodium salt of 4-carboxyphenylboronic acid (Hcpb) and lanthanide ions (Pr−Nd, Sm−Lu, and Y) led to a family of lanthanide-based coordination polymers with general chemical formula $\{[Ln(cpbOH)(H_2O)_2](cpb)\}_\infty$. Structural characterizations were ensured by single-crystal X-ray diffraction and solid-state NMR spectroscopy (^{11}B, ^{13}C, and ^{89}Y). This family of compounds constitutes the first example of lanthanide-based coordination polymers involving 4-carboxyphenylboronic acid as ligand. To evaluate their potential usefulness, luminescent and magnetic properties of some of the compounds that constitute this family were explored. From a magnetic point of view, the Yb(III) compound is the more promising. On the other hand, upon UV irradiation (λ_{exc} = 303 nm) ligand phosphorescence is quite intense and offers a sizable blue component to emission spectra. This is quite unusual and can constitute an asset as far as white emission is targeted. Moreover, luminescence properties of these compounds are highly temperature-dependent, and some of them seem promising as molecular thermometers.

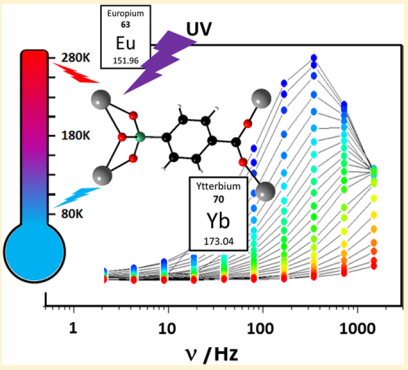

INTRODUCTION

For more than a decade, lanthanide-based coordination polymers have attracted great attention because of their fascinating topologies[1,2] coupled with their potential applications in gas storage,[3−10] catalysis,[11] separation,[12] luminescence,[13−22] or molecular magnetism.[23−25] Because lanthanide ions are hard Pearson acids,[26,27] ligands with oxygen donor atoms have been extensively studied.[28,29] Among these ligands, special attention has been paid to benzene-polycarboylates[30] and more particularly to terephthalate,[13,31−37] which, in association with lanthanide ions, has been proved to lead to efficient tags for fight against counterfeiting.[38−40] Our group is involved for many years in the synthesis and the study of lanthanide-based coordination polymers[41] and the search of new ligands that could lead to new structural network and/or new physical properties is a continuous concern. Therefore, we decided to take an interest in lanthanide-based coordination polymers with 4-carboxyphenylboronic acid as ligand (Scheme 1). Actually, this rodlike ligand can present a structuring effect via π-stacking and hydrogen bonds. It presents two functions with donor oxygen atoms, and it can act as an antenna for luminescent properties. Furthermore, because of their low toxicity and their ultimate degradation into the environmentally friendly boric acid, boronic acids can be regarded as "green compounds". Actually, in the past two decades, the status of boronic acids in chemistry has risen from rather neglected compounds to a prime class of synthetic intermediates in chemistry and medicine.[42]

Scheme 1. 4-Carboxyphenylboronic Acid (Hcpb)

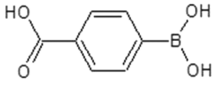

Notice that 4-carboxyphenylboronic acid (Hcpb) presents both the acidic character of a Bronsted acid (carboxylic group) and the Lewis acidic character because of the vacant p orbital of the boron atom[43] (see Scheme 2). This particularity could lead to original structural properties.

Some lanthanide complexes with boronic acids have been studied in solution,[44−46] but to the best of our knowledge no crystal structure has been reported so far.[47,48] Moreover, coordination polymers with 4-carboxyphenylboronic acid as ligand are very rare,[49] and none of them involve lanthanide ions. In this paper, we wish to describe the first family of lanthanide-based coordination polymers with a boronic acid as ligand. Its luminescent and magnetic properties are also studied to estimate the interest of such compounds for potential applications.

EXPERIMENTAL SECTION

Synthesis of the Microcrystalline Powders. 4-Carboxyphenylboronic acid was purchased from Sigma-Aldrich and used without further purification. Its sodium salt is prepared by addition of 1 equiv of sodium hydroxide to a suspension of 4-carboxyphenylboronic acid in deionized water. Then pH is adjusted to 7 by an additional amount of sodium hydroxide. Overall, the relative ratio Hcpb/NaOH is 1:1.2. The obtained clear solution is then evaporated to dryness. The resulting solid is put in suspension in a small amount of ethanol. The mixture is stirred

Received: March 20, 2015
Published: May 14, 2015

DOI: 10.1021/acs.inorgchem.5b00635
Inorg. Chem. 2015, 54, 5534−5546

Scheme 2. Acid/Base Equilibriums of 4-Carboxyphenylboronic Acid in Water

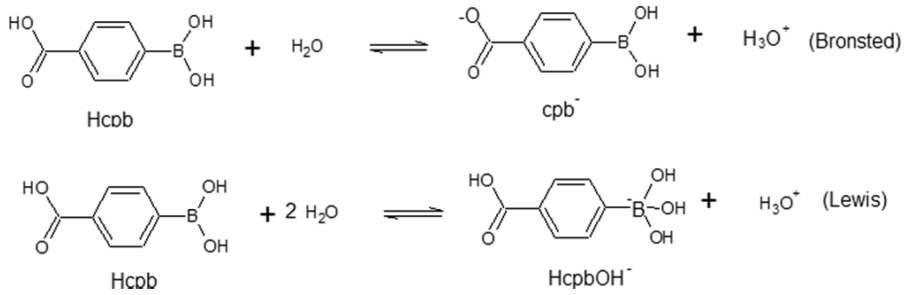

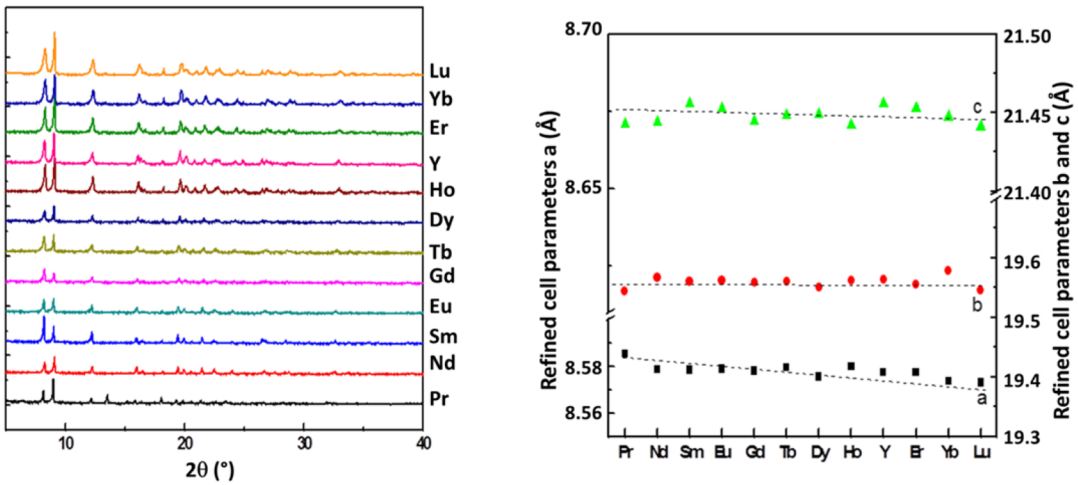

Figure 1. (left) Experimental X-ray diffraction diagrams of the microcrystalline powders obtained with Ln = Pr−Nd, Sm−Er, Yb−Lu, and Y. (right) Fitted cell parameters, versus the ionic radius of the involved lanthanide ion. Ionic radii are for eight coordinated ions.[51]

and refluxed for 1 h. Upon addition of ethoxyethane precipitation occurs. After filtration and drying, a white powder of sodium salt of 4-carboxyphenylboronic acid is collected in 90% yield. Thermogravimetric analysis reveals that the salt is hemihydrated (Supporting Information, Figure S1). Elemental analysis of $C_7H_7BO_{4.5}Na$ (MW = 197 g·mol^{-1}): Calculated (Found): C 42.7% (42.5%) ; H 3.6% (3.7%) ; B 5.5% (5.6%) ; O 36.6% (36.7%) ; Na 11.6% (11.5%).

UV−vis absorption spectra of aqueous solutions of this salt were recorded (Supporting Information, Figure S2), and the molar extinction coefficient was calculated: ε_{max} = 1100 L mol^{-1} cm^{-1} (see Supporting Information, Figure S3).

Hydrated lanthanide chlorides are prepared from the corresponding oxides according to literature.[50] Lanthanide oxides were purchased from Ampere company and used without further purification.

Microcrystalline powders of the coordination polymers are obtained by mixing stoichiometric amounts of lanthanide chloride in water with the sodium salt of 4-carboxyphenylboronic acid. Precipitations progressively occur. The mixtures are stirred for 40 min at room temperature before the precipitates are filtered and dried in air. The yields of the reactions are close to 90%. Results of the elemental analysis are listed in Supporting Information, Table S1.

The obtained microcrystalline powders were assumed to be isostructural, on the basis of their X-ray powder diffraction diagrams for lanthanide comprised of Pr−Nd, Sm−Lu, and Y (Figure 1).

Synthesis of the Single Crystals. Tetramethyl orthosilicate (TMOS) was purchased from Acros Organics and jellified according to established procedures.[52−54] Dilute solutions of Ln(III) chloride (0.1 mol L^{-1}) and sodium salt of 4-carboxyphenylboronic acid (0.1 mol L^{-1}) were allowed to slowly diffuse through this gel medium in U-shaped tubes. After a few weeks hexagonal platelike single-crystals suitable for X-ray diffraction analysis were obtained in the tubes that had been filled with a 7.5% gel (expressed in weight percent) with all lanthanide ions. Alternatively, single crystals of poorer quality can be obtained by slow evaporation of the filtrates obtained during the synthesis of the microcrystalline powders. The single crystals that were chosen for recording the X-ray diffraction data were obtained by slow diffusions in U-shaped tubes with the Tb^{3+} ion.

X-ray Powder Diffraction. The diagrams were collected using a Panalytical X'Pert Pro diffractometer with a X'Celerator detector. The typical recording conditions were 45 kV, 40 mA for Cu Kα (λ = 1.542 Å), the diagrams were recorded in θ/θ mode in 60 min between 5° and 75° (8378 measurements) with a step size of 0.0084° and a scan time of 50s. The calculated patterns were produced using the Powdercell and WinPLOTR software programs.[55−57] For Pattern indexing, the extractions of the peak positions were executed via the WinPLOTR software. The pattern indexing was performed by the program McMaille,[58] and the refinement of the unit-cell parameters by means of the Chekcell program, which is a modified version of Cellref from CRYSFIRE suite.[59]

Thermally dependent X-ray diffraction experiments were performed with a Panalytical X'Pert Pro diffractometer equipped with an X'celerator detector using Cu Kα_1 radiation in the 5−75° 2θ range. Heating of the samples (from room temperature to 1000 °C) was performed using an Anton Paar HTK 1200 furnace under nitrogen atmosphere.

Thermal Analyses. Thermogravimetric and thermodifferential analyses were performed in platinum crucibles under a nitrogen atmosphere between room temperature and 1000 °C with a heating rate of 5 °C min^{-1} using a PerkinElmer Pyris-Diamond thermal analyzer. At the end of the experiments, the compounds were maintained for 1 h at 1000 °C under air atmosphere to complete the combustion.

Single Crystal X-ray Diffraction Data. Crystals were sealed in glass capillaries for X-ray single-crystal data collection to avoid potential dehydration. Single crystals were mounted on a Nonius Kappa CCD diffractometer with Mo Kα radiation (λ = 0.710 73 Å). The crystal data collection was performed at room temperature.

The crystal structure was solved by direct methods using the SIR97 program[60] and then refined with full matrix least-squares methods based on F^2 (SHELX-97)[61] with the aid of WINGX program.[62] All non-hydrogen

DOI: 10.1021/acs.inorgchem.5b00635
Inorg. Chem. 2015, 54, 5534−5546

atoms were refined anisotropically using the SHELXL program. Hydrogen atoms bound to the organic ligand were localized at ideal positions. Hydrogen atoms of water molecules were not localized. Hydrogen atoms of the boronic functions were localized by Fourier difference and refined, but both hydrogen atoms of the $B(OH)_2$ function of the cpb^- free ligand were blocked. Absorption corrections were performed using the facilities[62−64] included in the WinGX program suite.[62] Crystal and final structure refinement data of the crystal structure are listed in Table 1. Additional crystallographic information is available in the Supporting Information.

Table 1. Crystal and Final Structure Refinement Data for $\{[Tb(cpbOH)(H_2O)_2](cpb)\}_\infty$

molecular formula	$TbO_{11}C_{14}H_{17}B_2$
system	Orthorhombic
a (Å)	8.5704(1)
b (Å)	19.5441(1)
c (Å)	21.4191(3)
V (Å^3)	3587.71(7)
Z	8
formula weight (g mol^{-1})	541.82
space group (No.)	*Pbca* (No. 61)
D_{calc} (g.cm^{-3})	1.98
μ (mm^{-1})	4
R (%)	3.8
R_W (%)	9.01
GOF	1.082
No. CCDC	962513

Solid-State Luminescent Measurements. Solid-state emission spectra were measured on a Horiba Jobin-Yvon Fluorolog III fluorescence spectrometer with a Xe lamp. Slit widths for excitation and emission were 2 nm for the Eu- and Tb-containing compounds and 5 nm for the Sm- and Dy-containing compounds. Most of the luminescence spectra were recorded between 450 and 750 nm at room temperature. Some of them were also recorded at 77 K using a coldfinger sample holder. The data were collected at every 0.5 nm with an integration time of 100 ms for each step. The quantum yield measurements were performed using a Jobin-Yvon integrating sphere ($\Phi = (E_c - E_a)/(L_a - L_c)$ with E_c being the integrated emission spectrum of the sample, E_a the integrated "blank" emission spectrum, L_a the "blank" absorption, and L_c the sample absorption at the excitation wavelength). Luminescence decays were also measured using this apparatus. Temperature-dependent luminescence measurements were performed using an Optistat CF2 cryostat from Oxford Instruments.

Comparative solid-state luminescence spectra were measured on a PerkinElmer LS-55 spectrometer between 450 and 750 nm under identical operating conditions and without turning the lamp off to ensure a valid comparison between the emission spectra. Reproducibility of the measurements as well as surface states of the samples (1.5 cm^2 pellets) were carefully checked. Slit widths for excitation and emission were 5 or 10 nm depending on the series of samples.

The solid-state luminescence spectrum of the Gd-containing compound was recorded at 77 K to obtain the energy levels of the lowest triplet state of the ligand (see Supporting Information, Figure S4).

Luminescence intensities of the samples expressed in Cd m^{-2} were measured with a Gigahertz-Optik X1−1 optometer with an integration time of 200 ms on 1.5 cm^2 pellets. The intensity of the UV flux, 2.5(1) W m^{-2}, was measured with a VilberLourmat VLX-3W radiometer.

UV−Visible Absorption Measurements. UV−vis absorption spectra were recorded on a PerkinElmer Lambda 650 spectrometer. Solid-state measurements were recorded using a 60 mm integrating sphere. Solid-state UV−vis absorption spectrum of the Gd-containing compound was recorded for estimating the energy of the lowest singlet excited state of the ligand (see Supporting Information, Figure S5). Liquid state measurements were performed for evaluating molar absorption coefficients of the ligand (see Supporting Information, Figure S3).

Colorimetric Measurements. The CIE (Commission Internationale de l'Eclairage) (x,y) emission color coordinates[65,66] were obtained using a MSU-003 colorimeter (Majantys) with the PhotonProbe 1.6.0 Software (Majantys). Color measurements: 2°, CIE 1931, step 5 nm, under 312 nm UV light. $X = k \times \int_{380nm}^{780nm} I_\lambda \times x_\lambda$, $Y = k \times \int_{380nm}^{780nm} I_\lambda \times y_\lambda$ and $Z = k \times \int_{380nm}^{780nm} I_\lambda \times z_\lambda$ with k constant for the measurement system, I_λ sample spectrum intensity, wavelength depending, x_λ, y_λ, z_λ trichromatic values $x = X/(X + Y + Z)$, $y = Y/(X + Y + Z)$ and $z = Z/(X + Y + Z)$. Mean xyz values are given for each sample, which act as light sources (luminescent samples). Standards from Phosphor Technology used, calibrated at 312 nm: red phosphor Gd_2O_2S/Eu (x = 0.667, y = 0.330) and green phosphor Gd_2O_2S/Tb (x = 0.328, y = 0.537)

For other excitation wavelengths than 312 nm colorimetric coordinates were calculated on the basis of emission spectra that were measured on a PerkinElmer LS-55 spectrometer. Each apparatus

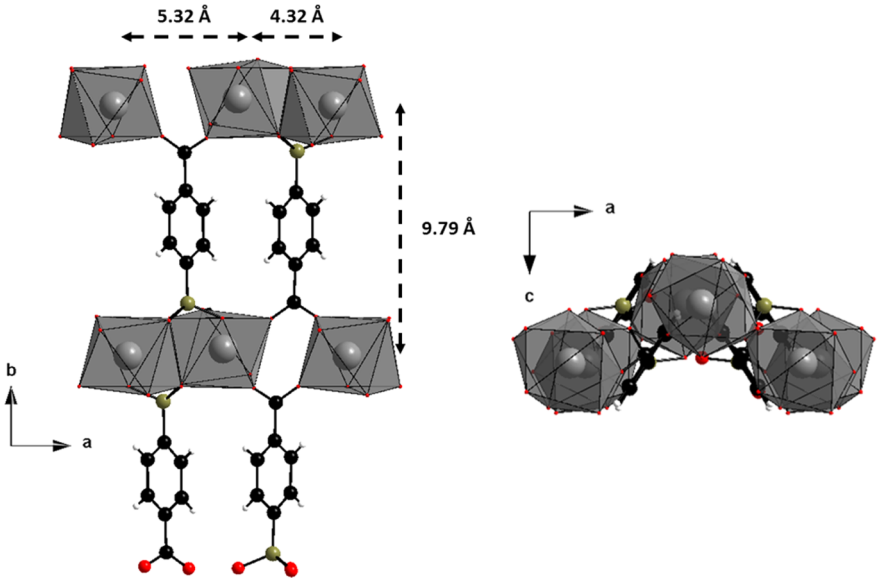

Figure 2. Projection views along the $\vec{c}$ (left) and $\vec{b}$ (right) axes of a molecular layer of $\{[Tb(cpbOH)(H_2O)_2](cpb)\}_\infty$. Tb^{3+} polyhedron were drawn. Hydrogen atoms of coordination water molecules were omitted for clarity.

DOI: 10.1021/acs.inorgchem.5b00635
Inorg. Chem. 2015, 54, 5534−5546

presents different geometries, which induces a little discrepancy between the results.

Solid-State NMR Spectroscopy. ^{11}B NMR (I = 3/2) experiments were performed at two different magnetic fields, 7 and 14 T, respectively, at frequencies of 96.29 and 192.55 MHz. We employed typical RF field strength of 45 kHz. Spectra were referenced with respect to boric acid in aqueous solution. The use of SPINAL64 proton decoupling is necessary to correctly observe the second order quadrupolar line shape of boron signals. Samples were packed either in 4 mm (7 T) or 2.5 mm rotors (14 T). Signals were processed using probe background signal subtractions and externally referenced with respect to aqueous boric acid.

^{13}C MAS spectra were acquired using a Bruker Avance III spectrometer equipped with a 14 T magnet. Spectra were acquired using cross-polarization (CP) from ^{1}H using a contact pulse duration of 5 ms (ramped 50−100% for ^{1}H), and SPINAL64 proton decoupling during acquisition with an RF field strength of ∼60 kHz and a recycle interval of 5 s. Samples were packed into 2.5 mm outer diameter rotors and rotated at a spinning rate of 10 kHz using a commercial probehead. ^{13}C spectra are referenced with respect to TMS.

^{89}Y CPMAS experiments were recorded at 14 T, using a low-gamma two channels 4 mm probe. Spectrum recorded at a MAS rate of 4 kHz. ^{89}Y MAS NMR spectra were acquired using cross-polarization (CP) from ^{1}H using a contact time of 5 ms (ramped for ^{1}H), SPINAL64 ^{1}H decoupling during acquisition with an RF field strength of ∼60 kHz and recycle interval of 3 s. Chemical shift scales are shown relative to 1 mol L^{-1} YCl_3 in aqueous solution.

Magnetic Measurements. All magnetic measurements were performed on pellets to avoid crystallite orientation of these very anisotropic materials. The alternating- and direct-current (ac and dc) magnetic susceptibility measurements were performed with an MPMS Quantum Design SQUID magnetometer between 2 and 300 K. These measurements were all corrected for the diamagnetic contribution as calculated with Pascal's constants.

RESULTS AND DISCUSSION

Compounds that constitute the family have general chemical formula $\{[Ln(cpbOH)(H_2O)_2](cpb)\}_\infty$. where Ln symbolizes a trivalent lanthanide ion (Pr−Nd, Sm−Lu, and Y). All of them can be obtained as microcrystalline powders. They are all isostructural. The crystal structure was solved on the basis of a Tb-containing single crystal, and the isostructurality of the other compounds was assumed on the basis of their powder X-ray diffraction patterns (Figure 1).

The crystal structure is two-dimensional and can be described as the superimposition of wavy planes that spread parallel to the $(\vec{a}, \vec{b})$ plane (see Figure 2). These layers can be described as Tb^{3+} dimeric chains that spread in the $\vec{a}$ direction. Tb−Tb distances between Tb^{3+} ions that belong to the same dimeric unit are 4.32 Å, while they are 5.32 Å for Tb^{3+} ions that belong to adjacent dimeric units. These inorganic chains are linked to each other by 4-carboxyphenylborate ligands that are aligned parallel to the $\vec{b}$ axis. The shortest distances between two Tb^{3+} ions that belong to adjacent inorganic chains is 9.79 Å.

Notice that the ligand involved in the molecular layer is dianionic ($cpbOH^{2-}$). Therefore, the bidimensional layers described above are cationic because there are only one Tb^{3+} ion and one $cpbOH^{2-}$ ligand in the asymmetric unit (see Figure 3). The overall neutrality is ensured by a free cpb^- ligand that is located between the molecular layers. Tb^{3+} ion is eight-coordinated by four oxygen atoms from two $B(OH)_3^-$ groups, two oxygen atoms from two carboxylates groups, and two oxygen atoms from coordination water molecules (see Figure 4 left). The coordination polyhedron of the Tb^{3+} ion is best described as a distorted square antiprism (D_{4d} site symmetry) as evidenced by SHAPE calculations[67] (SHAPE Factor is D_{4d} = 2.805, second closest site symmetry is C_{2v}= 2.977).

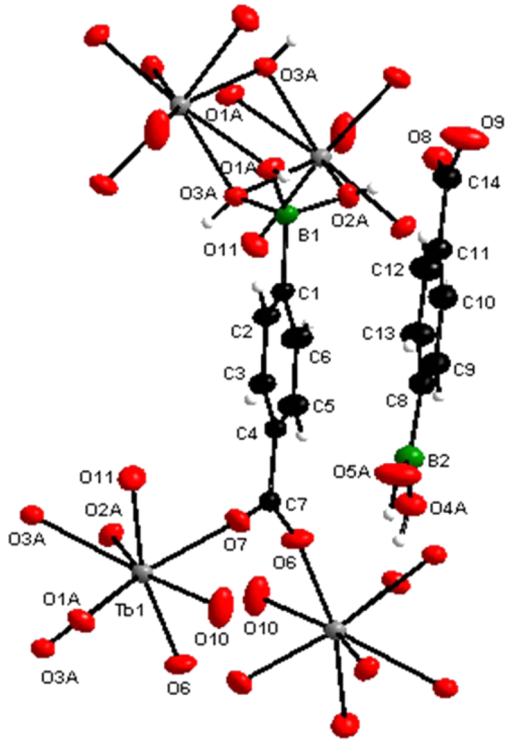

Figure 3. Extended asymmetric unit with the labeling scheme of $\{[Tb(cpbOH)(H_2O)_2](cpb)\}_\infty$.

The $cpbOH^{2-}$ ligand links four Tb^{3+} ions. Its carboxylate group bridges two Tb^{3+} ions by two μ_2-O atoms (see Figure 4, right). On the other hand, the $B(OH)_3^-$ group bridges two Tb^{3+} ions by two μ_2-OH groups and one μ_3-OH group (see Figure 4, right). There is no crystallization water molecule in the framework whose stability is ensured by a complex network of hydrogen bonds as already observed in the crystal structure of Hcpb.[68]

Additionally, cell parameters of the Er-based compound were measured both at room temperature and 100 K. No crystallographic phase transition was observed, and only a moderate cell contraction (∼1%) occurred. Therefore, it can be assumed that there is almost no influence of the temperature on the crystal structure.

Solid-State Nuclear Magnetic Resonance Spectroscopy. It can be noticed that the acido-basic state of the ligand plays a key role in this structural model. Unfortunately, IR spectroscopy was not fully informative. Therefore, to support our structural model, some ^{11}B, ^{13}C, and ^{89}Y solid-state NMR spectra of $\{[Y(cpbOH)(H_2O)_2](cpb)\}_\infty$ were recorded. We also intended to evaluate, in this particular case, the sensitivity of NMR techniques to small structural changes in the prospect of future work on isostructural solid solutions. NMR results are fully consistent with the X-ray structural elucidation.

^{13}C and ^{89}Y CPMAS results (Supporting Information, Figures S6 and S7) are consistent with the crystallographic structure of the material. ^{89}Y NMR spectrum presents a single narrow line at 26.2 ppm as expected for one rare earth crystallographic position. ^{13}C NMR spectrum presents signals between 124 and 141 ppm that correspond to the aromatic carbons and two signals at 173 and 178 ppm that we can tentatively attribute to different carboxylate signals.

^{11}B NMR spectroscopy is more informative and certainly a valuable tool in the prospect of structural studies of solid solutions. The boron spectra (Figure 5) exhibit very clearly two

DOI: 10.1021/acs.inorgchem.5b00635
Inorg. Chem. 2015, 54, 5534−5546

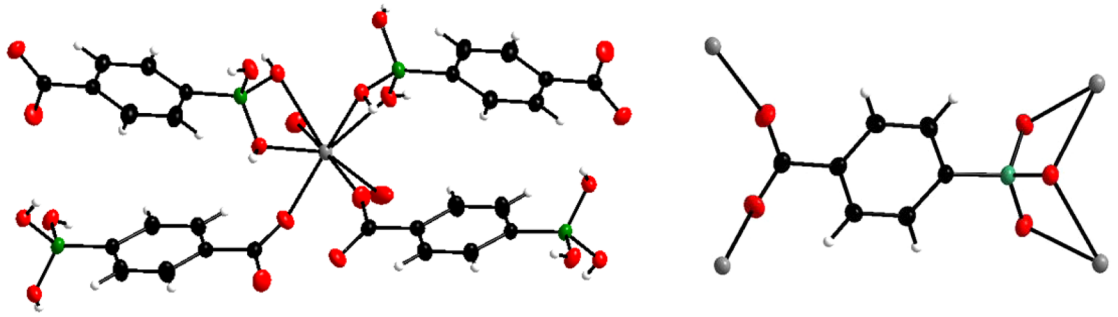

Figure 4. (left) Surrounding of the Tb^{3+} ion in $\{[Tb(cpbOH)(H_2O)_2](cpb)\}_\infty$. (right) Coordination mode of the $cpbOH^{2-}$ ligand.

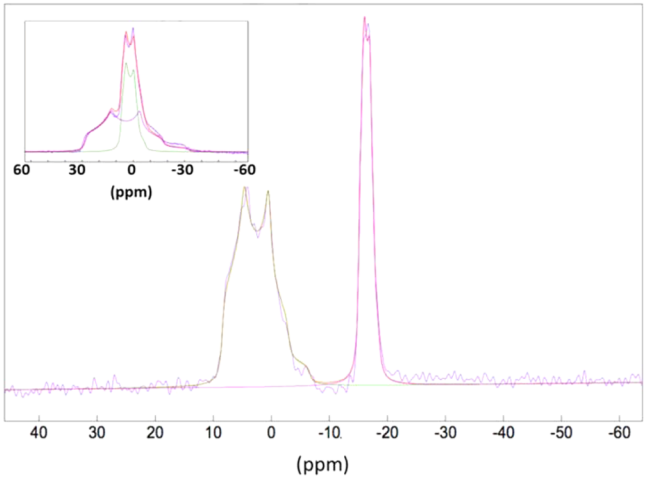

Figure 5. ^{11}B MAS NMR spectra of $\{[Y(cpbOH)(H_2O)_2](cpb)\}_\infty$ recorded at 14 T and (inset) 7 T under proton decoupling (spectra referenced to aqueous boric acid). Comparison between experimental spectra and the corresponding fit made using the Dmfit program.[69] The spectra at two different fields were fitted using the same parameters presented in Table 2.

signals presenting very substantial differences of second-order quadrupolar interactions. To get reliable values of quadrupolar parameters (quadrupolar coupling constants C_Q and asymmetry parameters), experiments were performed at two magnetic field and under proton decoupling. Proton decoupling allows significant improvement of the measurements of quadrupolar parameters, particularly for the signal presenting a large C_Q value. Data recorded at two magnetic fields (7 and 14 T) were fitted[69] using the same set of parameters (isotropic chemical shift and quadrupolar parameters). Results are presented in Table 2.

Table 2. ^{11}B NMR Parameters Extracted from Simultaneous Fit (Dmfit[69]) of ^{11}B MAS Spectra of $\{[Y(cpbOH)(H_2O)_2](cpb)\}_\infty$ under Proton Decoupling

	isotropic chemical shift[a] (ppm)	quadrupolar coupling constant C_Q (MHz)	asymmetry parameter
Boron 2	9.2	3.016	0.44
Boron 1	−14.92	1.480	0.42

[a]Recorded at magnetic field strength of 7 and 14 T (spectra referenced to aqueous boric acid).

Considering the local environment of boron atoms in the structure, we can attribute the signal with the largest quadrupolar interaction to the Boron 2 crystallographic position (atoms in triangular environment) and the smallest one to the Boron 1 atoms in tetrahedral environment.

Thermal Stability. The thermal behavior of $\{[Tb(cpbOH)(H_2O)_2](cpb)\}_\infty$ was also investigated by temperature-dependent powder X-ray diffraction (TDXD) and thermal analyses (TGA-TDA). TDXD measurements (Figure 6) show that the crystal

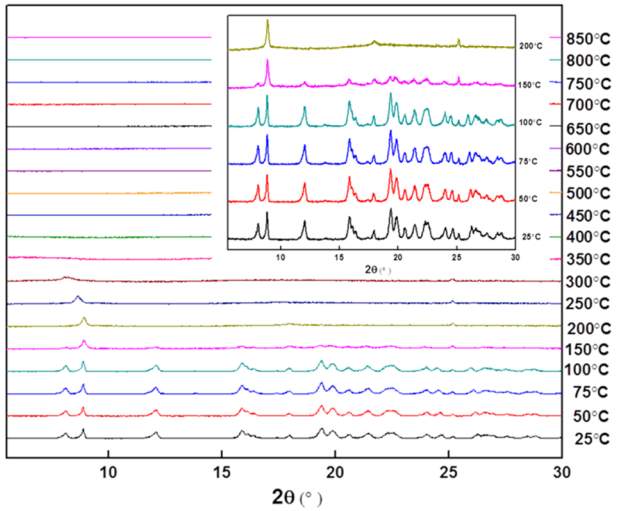

Figure 6. TDXD diagrams of $\{[Tb(cpbOH)(H_2O)_2](cpb)\}_\infty$ between room temperature and 850 °C. (inset) Between room temperature and 200 °C.

structure is unchanged from room temperature to 150 °C. Then the crystal structure collapses, and the powder becomes amorphous.

Thermal analyses (Supporting Information, Figure S8) show a first weight loss at 150 °C. This weight loss (13.6%) was

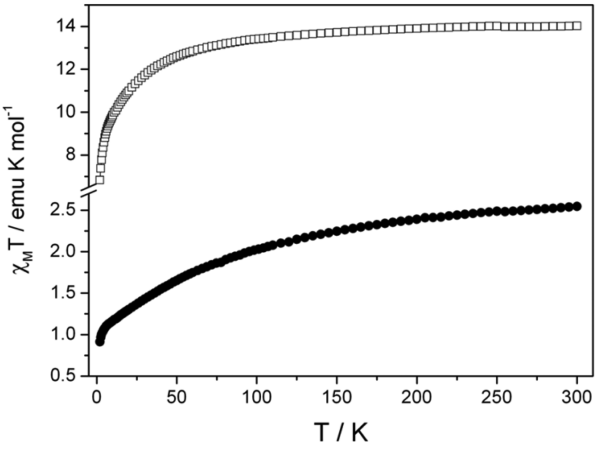

Figure 7. Temperature dependence of $\chi_M T$ for the Dy (squares) and Yb derivative (dots) of the $\{[Ln(cpbOH)(H_2O)_2](cpb)\}_\infty$ family.

DOI: 10.1021/acs.inorgchem.5b00635
Inorg. Chem. 2015, 54, 5534−5546

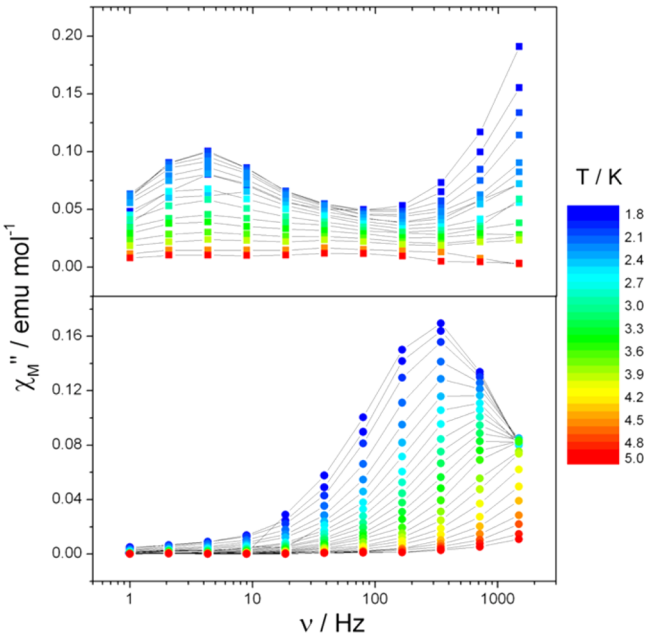

Figure 8. Frequency dependence of the out-of phase component of the magnetic susceptibility (χ_M'') for $\{[Dy(cpbOH)(H_2O)_2](cpb)\}_\infty$ (upper) and $\{[Yb(cpbOH)(H_2O)_2](cpb)\}_\infty$ (lower) between 1.8 and 5 K.

attributed to the removal of four water molecules (calc. 13.3%): Two coordination water molecules and two water molecules produced by the dehydration of the boronic functions.[43] Then a second weight loss is observed between 400 and 600 °C that was attributed to the decomposition of the ligand. These experiments demonstrate that this compound is thermally stable up to 150 °C, which constitutes an asset as far as potential applications are targeted.

Magnetic Measurements. The ac and dc magnetic measurements were performed to evaluate the capability of some derivatives of the $\{[Ln(cpbOH)(H_2O)_2](cpb)\}_\infty$. family to behave as single molecule magnets (SMMs).[70] SMMs are molecules that behave as magnets but with a magnetic bistability that has a molecular origin.[71] They thus offer new perspectives for a wide range of applications such as data storage,[72] molecular spintronics,[73,74] quantum computing,[75] etc. Given the square antiprism coordination environment of the lanthanide ion in the reported family, the Dy^{III}- and Yb^{III}-based compounds are the most suited derivatives to observe SMM properties.[76]

$\chi_M T$ versus T curves were measured by dc magnetometry (Figure 7) on Dy(III) and Yb(III) derivatives, and room-temperature values of $\chi_M T$ of 14.07 and 2.54 emu K mol^{-1} were observed for Dy^{III} and Yb^{III} derivatives, respectively. This is in agreement with what is expected for the corresponding isolated ions (Dy^{III}: $J = 15/2$, and $g_j = 4/3$; Yb^{III}: $J = 7/2$ and $g_j = 8/7$).[77] At lower T, all $\chi_M T$ values decrease as a consequence of the progressive depopulation of the m_J sublevels[77] (Figure 7 and Supporting Information, Figure S9). Evaluation of the coupling between the anisotropic lanthanides ions is complicated by this temperature dependence of the m_J population that induces thermal variation of several order of magnitude higher than the coupling itself. Moreover in our case, two interaction pathways must be considered: one through the carboxylic moiety (O7−C7−O6) that bridges two Ln^{III} ions and another one through the three OH^- moieties (O1A, O3A) at the other extremity of the ligand. Consequently, tentative fits of the $\chi_M T$ versus T curve considering two magnetic interactions ($J1$, $J2$) at low temperature provide senseless values, letting us suspect that these interactions are extremely small.

The ac magnetic measurements were performed on both derivatives (Figures 8 and Supporting Information, Figures S10−S14) to estimate their capabilities to behave as SMMs. No χ_M'' signals were detected, and zero-field fast tunneling (quantum tunneling) is suspected to hamper magnetic slow relaxation, which is commonly seen on similar compounds[78] (Supporting Information, Figure S11). However, as a small dc field is applied to remove degeneracy of m_J sublevels, clear χ_M'' signal is observed (Figure 8).

Optimum dc fields are found to be 2200 and 1600 Oe for Dy^{III} and Yb^{III} derivative, respectively (Supporting Information, Figure S10). Frequency dependence of χ_M'' is then observed between 1.8 and 5 K for both derivatives. For $\{[Dy(cpbOH)(H_2O)_2](cpb)\}_\infty$ two relaxation regimes are visible, and only the slower one is investigable. For this regime, temperature dependence of the magnetic relaxation is very small, and the external dc field only promotes a slow quantum tunneling regime for the relaxation. More interesting is $\{[Yb(cpbOH)(H_2O)_2](cpb)\}_\infty$ for which clear frequency dependence is observed that witnesses for a thermally activated magnetic slow relaxation. Consequently χ_M'' versus frequency curves can be fitted considering an Arrhenius law and the relaxation time (Supporting Information, Tables S2 and S3) is $\tau = \tau_0 \times \exp(\Delta/k_B T)$, where τ_0 is the characteristic relaxation time and Δ is the energy barrier that the molecule must overcome to relax[71] (Figure 9). Extracted values are $\tau_0 = 2.88 \times 10^{-5}$ s and $\Delta = 6.5$ K. For comparison the

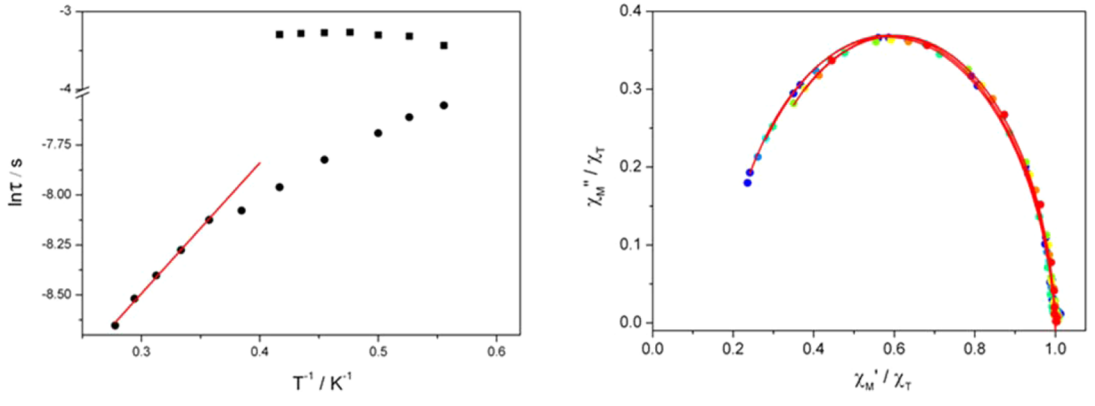

Figure 9. (left) Arrhenius plots of the relaxation times extracted for $\{[Dy(cpbOH)(H_2O)_2](cpb)\}_\infty$ (■) and $\{[Yb(cpbOH)(H_2O)_2](cpb)\}_\infty$ (●) with linear best fit (red). (right) Argand plot for $\{[Yb(cpbOH)(H_2O)_2](cpb)\}_\infty$ with some of the best fits (red).

DOI: 10.1021/acs.inorgchem.5b00635
Inorg. Chem. 2015, 54, 5534−5546

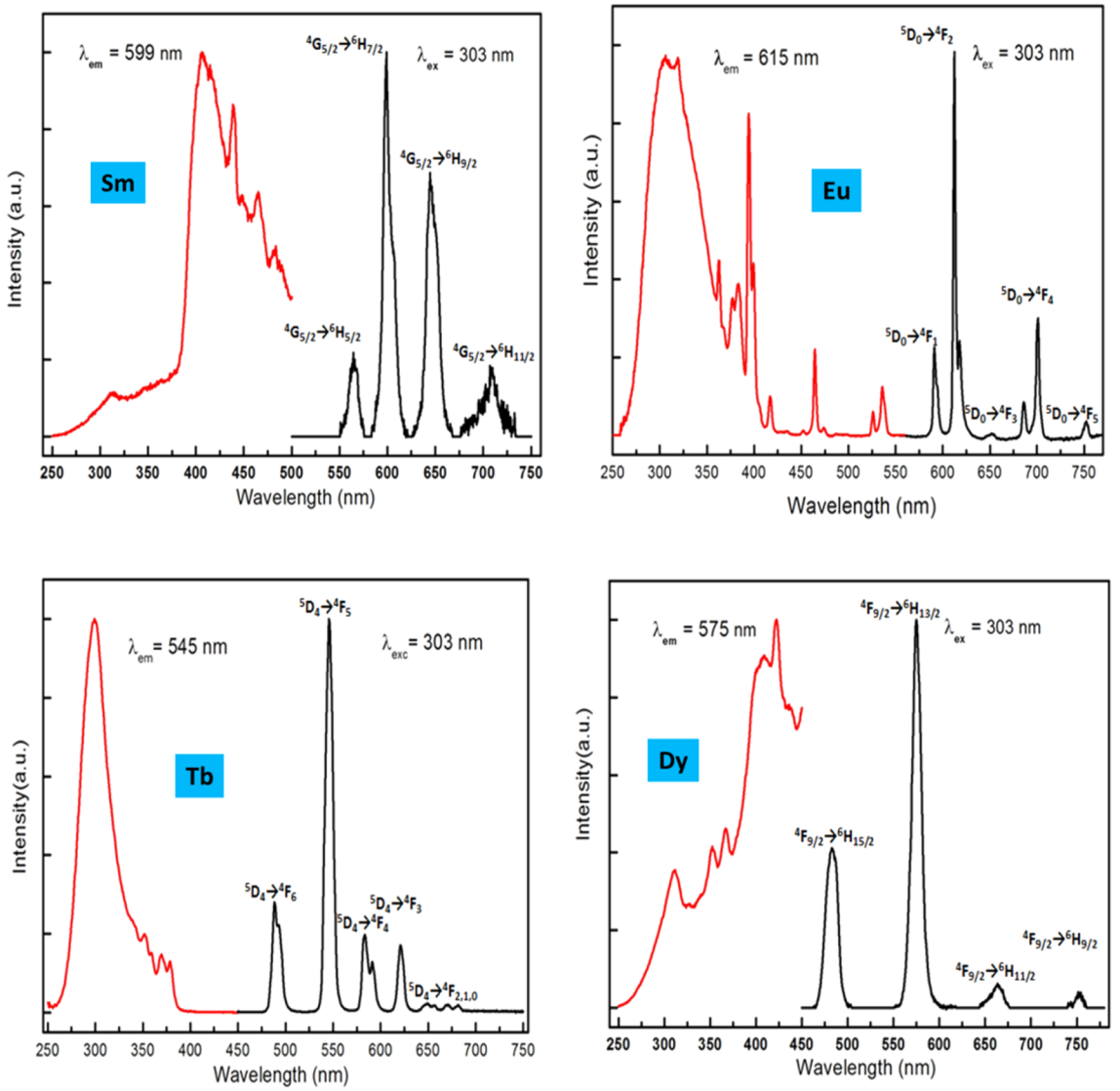

Figure 10. Excitation and emission spectra for $\{[Ln(cpbOH)(H_2O)_2](cpb)\}_\infty$ where Ln = Sm–Dy except Gd.

Dy derivative relaxes with $\tau_0 = 3.9 \times 10^{-2}$ s but with an energy barrier that is almost zero.

The distribution of the relaxation time of a sample can be characterized by plotting χ_M'' versus χ_M' in an Argand plot (Figure 9). The resulting curves can be fitted with the Debye model and $\chi(\omega) = \chi_S + (\chi_T - \chi_S)/(1 + (i\omega\tau)^{1-\alpha})$ in which χ_T and χ_S are the isothermal and adiabatic susceptibility respectively, ω the frequency of the ac field and α the parameter that accounts for the distribution of the relaxation times.[79] Consequently $\alpha = 0$ corresponds to a unique relaxation time (expected for an ideal SMM), and $\alpha = 1$ corresponds to an infinite distribution of the relaxation time (expected for a spin-glass).[80] For $\{[Yb(cpbOH)(H_2O)_2](cpb)\}_\infty$ α is ~0.06 at 1.8 K, which is an excellent agreement with a SMM-like behavior. Moreover $1 - (\chi'_M/\chi'_M T)$ is close to 0.85 (Supporting Information, Table S4) meaning that a very significant fraction of the sample is concerned by the magnetic slow relaxation.

Consequently on the $\{[Ln(cpbOH)(H_2O)_2](cpb)\}_\infty$ family the Yb derivative possesses clearly more significant SMM properties that its Dy analogue, which is quite rare in the library of Ln-based SMMs.[78] This is probably due to the distortion of the coordination polyhedron around the lanthanide that is far from an ideal D_{4d} symmetry. Thus, this deformation may offer an organization of the electrostatic surrounding of the lanthanide that favors the "prolate" nature of the Yb^{III} ion over the "oblate" one of the Dy^{III}.[81]

Solid-State Luminescence. Solid-state luminescence spectra were recorded for lanthanide-based compounds (Ln = Sm–Dy). It is well-known that one of the most important processes that has influence on the luminescent properties of the Ln^{III} ions in lanthanide-based coordination compound is the intramolecular transfer between the triplet state of the ligand and the lanthanide energy level. The lowest excited singlet and triplet states were estimated, respectively, by referring to the wavelength of the UV–vis absorbance edge (325 nm ≈ 30 750 cm^{-1}) and to the shortest wavelength phosphorescent band (400 nm ≈ 25 000 cm^{-1}) of the Gd-containing compound[82−85] (see Supporting Information, Figures S4 and S5). According to Reinhoudt's empirical rules[86] the intersystem crossing process becomes effective when $\Delta E(^1\pi\pi^* - ^3\pi\pi^*)$ is at least 5000 cm^{-1}. In the present case, the gap between the singlet and the triplet excited states (5750 cm^{-1}) is favorable for an efficient intersystem crossing process.

DOI: 10.1021/acs.inorgchem.5b00635
Inorg. Chem. 2015, 54, 5534–5546

Table 3. Overall Luminescent Quantum Yields and Observed Lifetimes for $\{[Ln(cpbOH)(H_2O)_2](cpb)\}_\infty$ where Ln = Sm–Dy except Gd

	Q_{Ln}^{ligand}	τ_{obs}
$\{[Sm(cpbOH)(H_2O)_2](cpb)\}_\infty$	0.11(1) %	5.3(1) μs
$\{[Eu(cpbOH)(H_2O)_2](cpb)\}_\infty$	6.0(6) %	0.217 ms
$\{[Tb(cpbOH)(H_2O)_2](cpb)\}_\infty$	46(4) %	0.843 ms
$\{[Dy(cpbOH)(H_2O)_2](cpb)\}_\infty$	0.19(2) %	1.9(2) μs

Actually, compounds that involve lanthanide ions that usually present luminescence in the visible region (Sm^{3+}, Eu^{3+}, Tb^{3+}, Dy^{3+}) can be excited at 303 nm (Figure 10). This indicates that 4-carboxyphenylboronic acid exhibits an antenna effect with respect to these ions.

When exposed under UV radiation (303 nm), these compounds emit visible light (Figure 10). The emission spectrum of the Sm-containing compound exhibits typical $^4G_{5/2} \rightarrow {}^6H_J$ ($J = 5/2–11/2$) and is dominated by the $^4G_{5/2} \rightarrow {}^6H_{7/2}$ and $^4G_{5/2} \rightarrow {}^6H_{9/2}$ transitions at 598 and 641 nm, respectively. The emission spectrum of the Eu-containing compound displays typical Eu^{3+} transitions ($^5D_0 \rightarrow {}^7F_J$ $J = 0–6$) and is dominated by the $^5D_0 \rightarrow {}^7F_2$ transition centered at 615 nm. The spectrum of the Tb-based compound features the characteristic Tb^{3+} $^5D_4 \rightarrow {}^7F_J$ ($J = 6–0$) transitions and is dominated by the $^5D_4 \rightarrow {}^7F_5$ transition at 545 nm. Finally, emission of the Dy-based compound arises from the Dy^{3+} $^4F_{9/2} \rightarrow {}^6H_J$ ($J = 15/2–9/2$) and is dominated by the $^4F_{9/2} \rightarrow {}^6H_{13/2}$ transition at 572 nm. Overall luminescent quantum yields (Q_{Ln}^{ligand}) and observed lifetimes (τ_{obs}) are listed in Table 3. The luminescent decay rates are monoexponential.

The weak luminescence of the Sm- and Dy-based compounds can be related to their small energy gaps.[87] Alternatively, the Eu- and Tb-based coordination polymers present quite sizable quantum yields. This is in agreement with Latva's empirical rules,[88,89] which predict that the energy of the lowest excited triplet state of the ligand (25 000 cm^{-1}) is supposed to favor good ligand-to-metal energy transfer without significant back-transfer for both the Eu- and the Tb-based compounds. Efficiency of the overall ligand-to-metal energy transfer (η_{sens}) is an important parameter. For lanthanide-containing compounds it is defined as the efficacy with which energy is transferred from the feeding levels of the ligand onto the lanthanide ion excited states:

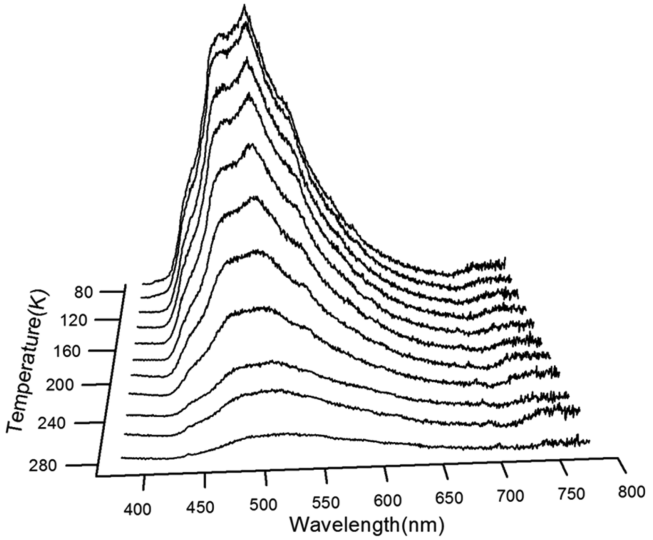

Figure 12. Emission spectra of $\{[Gd(cpbOH)(H_2O)_2](cpb)\}_\infty$ vs temperature under UV radiation (λ_{exc} = 303 nm).

$$Q_{Ln}^{ligand} = \eta_{sens} \times Q_{Ln}^{Ln} = \eta_{sens} \times \frac{\tau_{obs}}{\tau_{rad}} \quad (1)$$

where Q_{Ln}^{Ligand} is the overall quantum yield upon ligand excitation, Q_{Ln}^{Ln} is the intrinsic quantum yield upon direct excitation of the lanthanide ion, τ_{obs} is the observed luminescent lifetime, and τ_{rad} is the radiative luminescent lifetime.[90,91] The luminescence lifetime and the intrinsic quantum yield were measured for the Eu-based coordination polymer[92] under an excitation wavelength that corresponds to an f–f transition that does not overlap significantly with the absorption band of the ligand: 395 nm ($^5D_3$ energy level for Eu^{3+}).[93,94] This leads to Q_{Ln}^{Ln} = 7.1(1)% and η_{sens} = 84.9%.

For Eu-containing compounds a simplified equation leads to the radiative lifetime:[95]

$$\frac{1}{\tau_{rad}} = A_{MD,0} \times n \times \left(\frac{I_{tot}}{I_{MD}}\right) \quad (2)$$

Where $A_{MD,0}$, a constant equal to 14.65 s^{-1}, is the spontaneous emission probability of the magnetic dipole $^5D_0 \rightarrow {}^7F_1$, n is the refractive index, I_{tot} is the integrated emission of the $^5D_0 \rightarrow {}^7F_J$

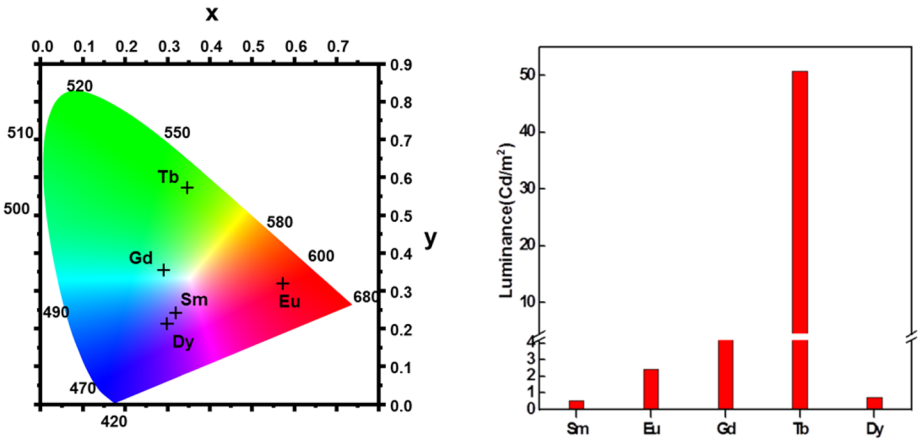

Figure 11. (left) Colorimetric data for $\{[Ln(cpbOH)(H_2O)_2](cpb)\}_\infty$ with Ln = Sm–Dy under UV radiation (λ_{exc} = 312 nm). (right) Luminance measurements for $\{[Ln(cpbOH)(H_2O)_2](cpb)\}_\infty$ with Ln = Sm–Dy under UV radiation (λ_{exc} = 312 nm). Numerical values are listed in Supporting Information, Table S5.

DOI: 10.1021/acs.inorgchem.5b00635
Inorg. Chem. 2015, 54, 5534–5546

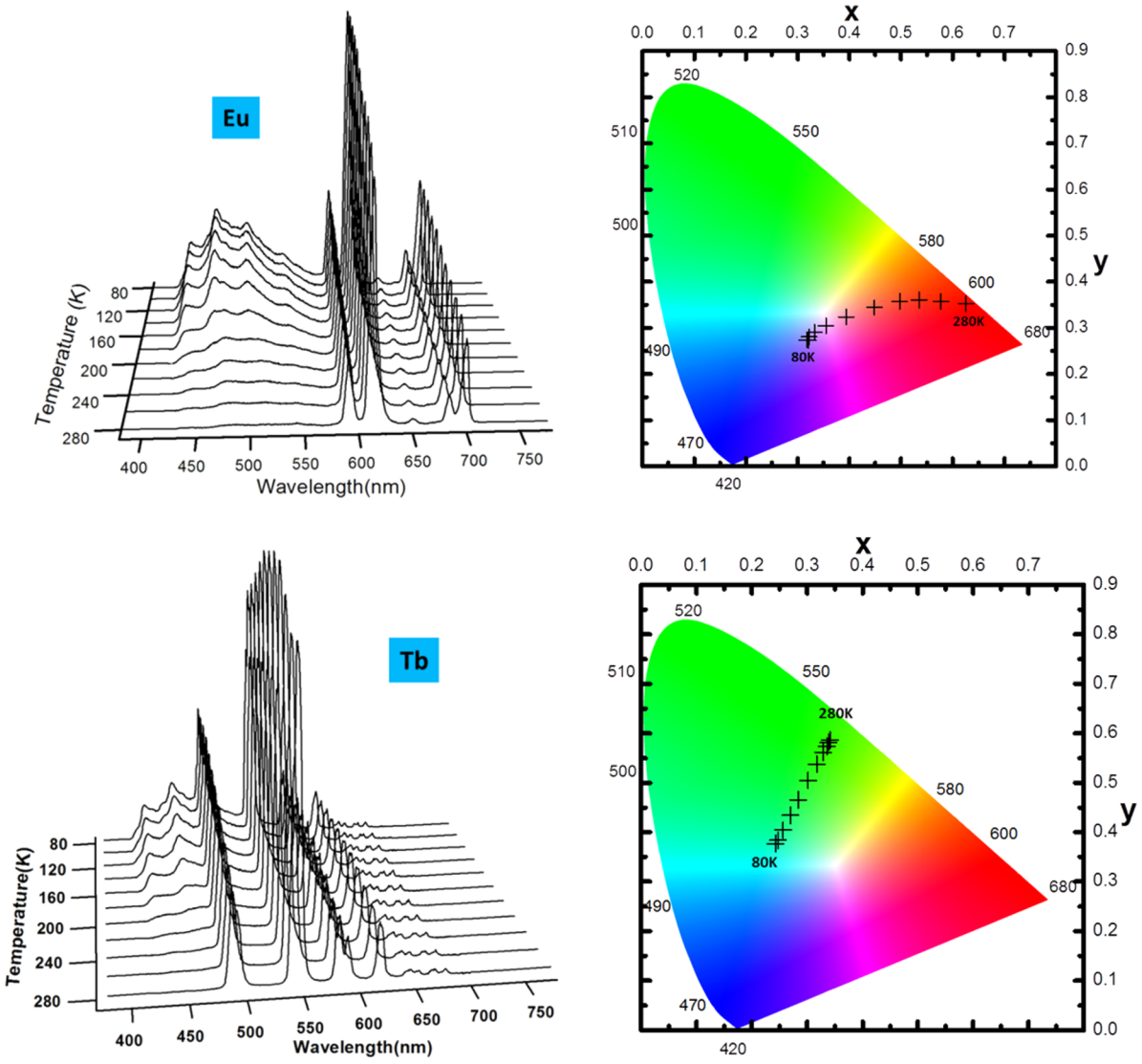

Figure 13. (upper) Emission spectra (left) and colorimetric coordinates (right) of $\{[Eu(cpbOH)(H_2O)_2](cpb)\}_\infty$ vs temperature under UV radiation (λ_{exc} = 303 nm). (bottom) Emission spectra (left) and colorimetric coordinates (right) of $\{[Tb(cpbOH)(H_2O)_2](cpb)\}_\infty$ vs temperature under UV radiation (λ_{exc} = 303 nm).

(J = 0−6) transitions, and I_{MD} is the integrated emission of the $^5D_0 \rightarrow {}^7F_1$ transition. Refractive index was estimated to 1.50 on the basis of known refractive indexes of similar compounds.[13] In this frame, Q_{Ln}^{Ln} = 7.0(1)% and η_{sens} = 85.0% values were obtained. Both set of values are in perfect agreement and show that ligand-to-Eu energy transfer is efficient. Unfortunately, it has not been possible to estimate the ligand-to-Tb energy transfer because relation 2 is only valid for Eu^{3+}-based compounds, and all usable f−f transitions overlap with the absorption band of the ligand for the Tb-containing compound. Nevertheless, these results indicate that ligand-to-metal energy transfer efficacy is not responsible for the significant difference between overall quantum yields that were measured for the Tb- and Eu-based compounds, respectively. This suggests that nonradiative deactivation of the Eu^{3+} is important. This can be related to the presence of two coordination water molecules and one chelating -$B(OH)_3$ group per lanthanide ion. Indeed, it is known that the luminescence of Eu^{3+} ions is more sensitive to deactivation by O−H oscillators than that of Tb^{3+} ions.[90]

Luminance and colorimetric coordinates under UV irradiation (λ_{exc} = 312 nm) were also measured for $\{[Ln(cpbOH)(H_2O)_2](cpb)\}_\infty$, where Ln = Sm−Dy (see Figure 11).

From these results it can be first noticed that the luminance of the Tb- and Eu-based compounds are quite sizable but lower than those measured for other coordination polymers that present comparable overall quantum yields.[96] This discrepancy between quantum yield and luminance can be related to the absorption ability of the ligand. Actually, the luminescence intensity depends on both the quantum yield and the molar absorption coefficient:

$$\Phi_{lum} \approx \varepsilon_\lambda \times Q_{Ln}^{ligand} \quad (3)$$

where Φ_{lum} is the luminescence intensity, Q_{Ln}^{ligand} is the overall quantum yield, and ε_λ is the molar absorption coefficient at the excitation wavelength.[97]

Because of the insolubility in solvents of these coordination polymers, their molar absorption coefficients could not be measured, which prevented us from estimating their luminescence intensity. Therefore, the molar absorption coefficient of

DOI: 10.1021/acs.inorgchem.5b00635
Inorg. Chem. 2015, 54, 5534−5546

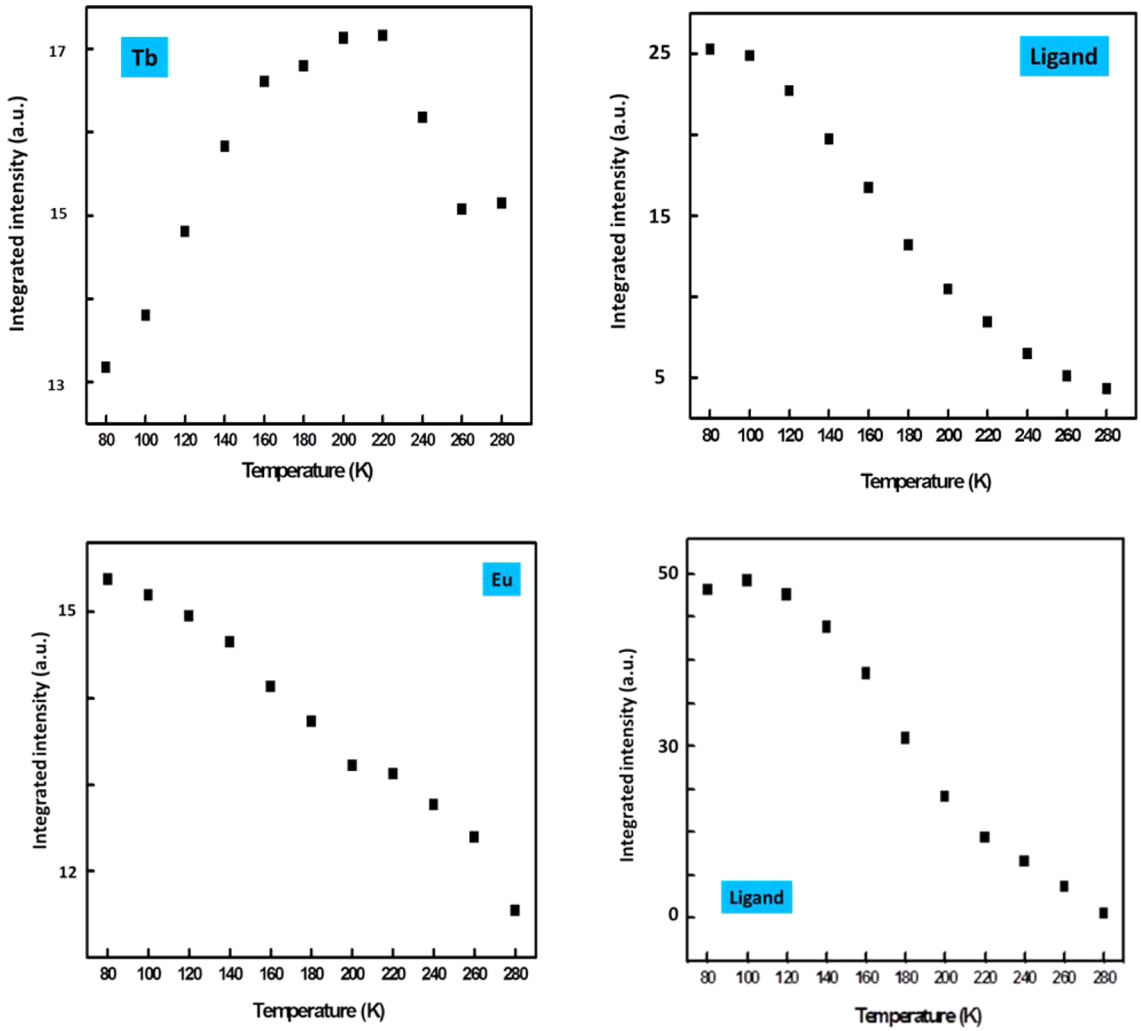

Figure 14. Integrated intensities of the emission spectra of $\{[Tb(cpbOH)(H_2O)_2](cpb)\}_\infty$ (upper) and $\{[Eu(cpbOH)(H_2O)_2](cpb)\}_\infty$ (lower) vs temperature under UV radiation (λ_{exc} = 303 nm). Contributions of the lanthanide ion (left) and of the ligand (right) are integrated separately.

the deprotonated ligand was calculated from dilute aqueous solutions of its sodium salt: $\varepsilon_{\lambda max}$ = 1110 L mol^{-1} cm^{-1} (see Supporting Information, Figure S3). This quite low value[96] explains the moderate luminance of these compounds.

Second, colorimetric coordinates of the Gd-, Sm-, and Dy-based compounds present a quite strong blue component. Obviously this is related to the luminescence of the ligand because Gd^{3+}-containing compounds cannot exhibit Gd^{3+}-induced luminescence under this excitation wavelength.

At last, the luminance of the Gd-based compound is unusually strong (even stronger than that of the Eu-containing compound). This suggests that the phosphorescence of the ligand could be used for obtaining the blue component that is often lacking in lanthanide-based coordination polymers. Moreover, triplet state phosphorescence is known for being highly thermo-dependent. Therefore, to support our assumption, we recorded emission spectra of the Gd-based compound versus temperature (Figure 12).

As expected, the ligand phosphorescence drastically increases as the temperature is lowered. This could be of interest as potential applications are targeted. Actually, temperature-dependent luminescence is a very common phenomenon that has already been used for developing molecular thermometer.[28,98,99] In previously described potential molecular systems the difference between the temperature-dependent luminescence of Eu^{3+} and Tb^{3+} ions in heteronuclear coordination polymers was studied. The more different they are the higher sensitivity can be. To evaluate the potential interest of the compounds that belong to this family of homonuclear coordination polymers, we compared the variation of the luminescence versus temperature of the ligand and of the lanthanide ion for both the Tb- and Eu-containing compounds. Emission spectra and colorimetric coordinates versus temperature are reported for both compounds in Figure 13.

From this figure it can first be noticed that the colorimetric coordinates vary over a large range with temperature. These measurements also confirm that these homonuclear coordination polymers are of interest as far as molecular thermometers are targeted. Actually, the luminescence of the ligand and one of the lanthanide ions varies differently with the temperature. For each spectrum, contributions that can be attributed to both the ligand phosphorescence and the lanthanide ion luminescence were estimated and integrated. Results for both compounds are reported in Figure 14.

Overall, all the intensities decrease as the temperature increases because of the thermal activation of nonradiative pathways. However, the decreases are not linear because they result in the combination of different mechanisms with different thermal behaviors (ligand deactivation, ligand-to-metal energy

DOI: 10.1021/acs.inorgchem.5b00635
Inorg. Chem. 2015, 54, 5534−5546

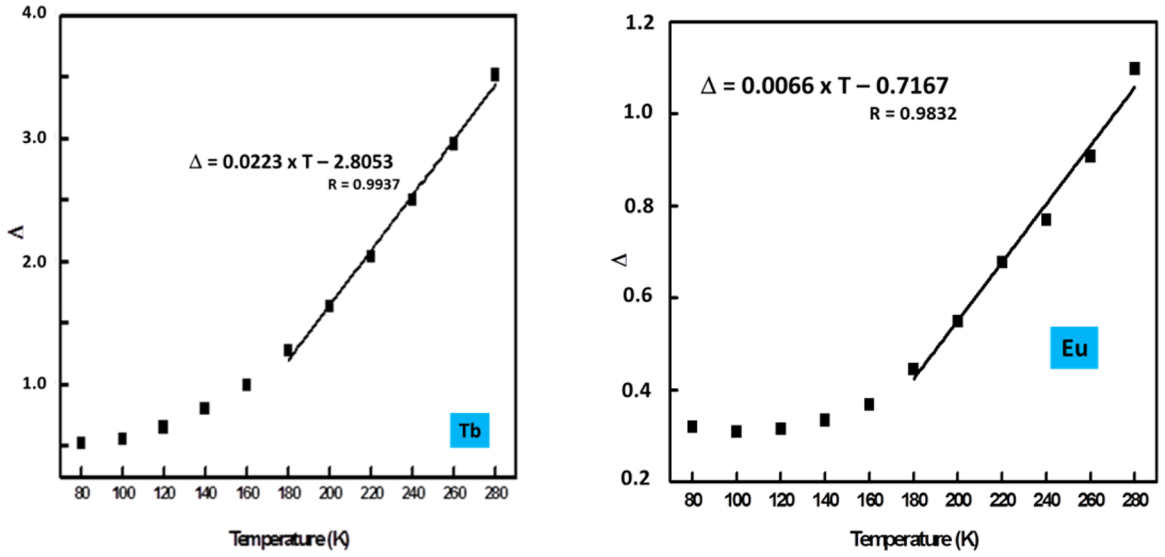

Figure 15. Parameter Δ vs T for $\{[Tb(cpbOH)(H_2O)_2](cpb)\}_\infty$ (left) and $\{[Eu(cpbOH)(H_2O)_2](cpb)\}_\infty$ (right) vs temperature under UV radiation (λ_{exc} = 303 nm).

transfer, metal deactivation, etc). To compare the potential efficiency as molecular thermometer of these compounds with already reported compounds a parameter Δ, which has been defined elsewhere,[99] was calculated:

$$\Delta = I_{Ln}/I_{Ligand} \quad (4)$$

where I_{Ln} is the integrated intensity of the contribution of the lanthanide ion to the emission spectrum and I_{Ligand} is the integrated intensity of the contribution of the ligand to the emission spectrum. It is noticeable that this parameter is independent of the emission scale and can be used for designing molecular thermometers that need no calibration. Results of the calculations are reported in Figure 15.

These results demonstrate that temperature can be correlated with the empirical parameter Δ between 200 and 300 K for both compounds. However, the Tb-based compound constitutes a much more sensitive thermometer (~2.2%) than the Eu-based one (~0.7%).[99] This value is quite sizable and can be compared with the best ones reported so far (3.5%).[99]

CONCLUSION AND OUTLOOK

The new family of compounds that have been described herein constitutes, to the best of our knowledge, the first example of lanthanide-based coordination polymers with a boronic acid as ligand. It has been structurally characterized by both single-crystal X-ray diffraction and solid-state NMR spectroscopy. Luminescent and magnetic properties have been explored and revealed to be quite promising: On one hand the Yb(III) derivative exhibits an SMM behavior; on the other hand, as far as luminescence is concerned, the strong and thermodependent phosphorescence of the compounds could constitute an asset. On the basis of these results, it appears that the study of heteronuclear isostructural compounds could reveal original and interesting properties. Our group is currently working along this line.

ASSOCIATED CONTENT

Supporting Information

Thermogravimetric analysis of $C_5H_7BO_{4.5}Na$; UV−vis absorption spectrum of an aqueous solution of $C_5H_7BO_{4.5}Na$; chemical analyses for $\{[Ln(cpbOH)(H_2O)_2](cpb)\}_\infty$ with Ln = Pr - Lu or Y; emission spectrum of $\{[Gd(cpbOH)(H_2O)_2](cpb)\}_\infty$ at 77 K; solid-state absorption spectrum of $\{[Gd(cpbOH)(H_2O)_2](cpb)\}_\infty$; absorbance versus concentration of aqueous solution of $Na(cpb)\cdot 0.5(H_2O)$; ^{13}C CPMAS spectrum of $\{[Y(cpbOH)(H_2O)_2](cpb)\}_\infty$; ^{89}Y CPMAS spectrum of $\{[Y(cpbOH)(H_2O)_2](cpb)\}_\infty$; field dependence of the magnetization for $\{[Dy(cpbOH)(H_2O)_2](cpb)\}_\infty$ and $\{[Yb(cpbOH)(H_2O)_2](cpb)\}_\infty$; frequency dependence of the out-of-phase component of the magnetic susceptibility (χ_M'') for $\{[Dy(cpbOH)(H_2O)_2](cpb)\}_\infty$ and $\{[Yb(cpbOH)(H_2O)_2](cpb)\}_\infty$ for several static magnetic fields; frequency dependence of the in-phase component of the magnetic susceptibility (χ_M'') for $\{[Dy(cpbOH)(H_2O)_2](cpb)\}_\infty$ and $\{[Yb(cpbOH)(H_2O)_2](cpb)\}_\infty$ between 1.8 and 5 K; frequency dependence of the out-of-phase component of the magnetic susceptibility (χ_M'') for, best fits and extracted values from the fitting of χ_M'' versus frequency curves of $\{[Yb(cpbOH)(H_2O)_2](cpb)\}_\infty$; frequency dependence of the out-of-phase component of the magnetic susceptibility (χ_M''), best fits and extracted values from the fitting of χ_M'' versus frequency curves of $\{[Dy(cpbOH)(H_2O)_2](cpb)\}_\infty$; Argand plots, best fits and extracted values from the Argand plot of $\{[Yb(cpbOH)(H_2O)_2](cpb)\}_\infty$; colorimetric coordinates and luminance for $\{[Ln(cpbOH)(H_2O)_2](cpb)\}_\infty$ with Ln = Sm−Dy. The Supporting Information is available free of charge on the ACS Publications website at DOI: 10.1021/acs.inorgchem.5b00635.

AUTHOR INFORMATION

Corresponding Authors

*E-mail: olivier.guillou@insa-rennes.fr.
*E-mail: carole.daiguebonne@insa-rennes.fr.

Notes

The authors declare no competing financial interest.

ACKNOWLEDGMENTS

The China Scholarship Council Ph.D. Program, a cooperation program with the French UT & INSA, is acknowledged for financial support. The Center of Diffraction X of the Univ. of Rennes1 (CDIFX) is acknowledged for single-crystal X-ray

DOI: 10.1021/acs.inorgchem.5b00635
Inorg. Chem. 2015, 54, 5534−5546

diffraction data collections. M. J. Guichard is acknowledged for his help during the spectroscopic data treatment.

REFERENCES

(1) Luo, Y.; Bernot, K.; Calvez, G.; Freslon, S.; Daiguebonne, C.; Guillou, O.; Kerbellec, N.; Roisnel, T. *CrystEngComm* **2013**, *15*, 1882−1896.
(2) Guillerm, V.; Weselinski, L.; Belmabkhout, Y.; Cairns, A. J.; D'Elia, V.; Wojtas, L.; Adil, K.; Eddaoudi, M. *Nat. Chem.* **2014**, *6*, 673−680.
(3) Yaghi, O. M.; Li, G.; Li, H. *Nature* **1995**, *378*, 703−706.
(4) Yaghi, O. M.; Li, H. L. *J. Am. Chem. Soc.* **1995**, *117*, 10401−10402.
(5) Eddaoudi, M.; Kim, J.; Rosi, N.; Vodak, D.; Wachter, J.; O'Keeffe, M.; Yaghi, O. M. *Science* **2002**, *295*, 469−472.
(6) Férey, G.; Serre, C.; Mellot-Draznieks, C.; Millange, F.; Surblé, S.; Dutour, J.; Margiolaki, I. *Angew. Chem., Int. Ed.* **2004**, *43*, 6296−6301.
(7) Férey, G.; Mellot-Draznieks, C.; Serre, C.; Millange, F. *Acc. Chem. Res.* **2004**, *38*, 217−225.
(8) Kustaryono, D.; Kerbellec, N.; Calvez, G.; Daiguebonne, C.; Guillou, O. *Cryst. Growth Des.* **2010**, *10*, 775−781.
(9) Luo, Y.; Calvez, G.; Freslon, S.; Daiguebonne, C.; Roisnel, T.; Guillou, O. *Inorg. Chim. Acta* **2011**, *368*, 170−178.
(10) Almeida Paz, F. A.; Klinowski, J.; Vilela, S. M. F.; Tome, J. P. C.; Cavaleiro, J. A. S.; Rocha, J. *Chem. Soc. Rev.* **2012**, *41*, 1088−1110.
(11) Lee, J.; Farha, O. K.; Roberts, J.; Scheidts, A.; Nguyen, S. T.; Hupp, J. T. *Chem. Soc. Rev.* **2009**, *38*, 1450−1459.
(12) Hamon, L.; Llewellyn, P. L.; Devic, T.; Ghoufi, A.; Clet, G.; Guillerm, V.; Pirngruber, G. D.; Maurin, G.; Serre, C.; Driver, G.; van Beek, W.; Jolimaitre, E.; Vimont, A.; Daturi, M.; Férey, G. *J. Am. Chem. Soc.* **2009**, *131*, 17490−17499.
(13) Freslon, S.; Luo, Y.; Calvez, G.; Daiguebonne, C.; Guillou, O.; Bernot, K.; Michel, V.; Fan, X. *Inorg. Chem.* **2014**, *53*, 1217−1228.
(14) Fan, X.; Freslon, S.; Daiguebonne, C.; Calvez, G.; Le Polles, L.; Bernot, K.; Guillou, O. *J. Mater. Chem. C* **2014**, 5510−5525.
(15) Luo, Y.; Zheng, Y.; Calvez, G.; Freslon, S.; Bernot, K.; Daiguebonne, C.; Roisnel, T.; Guillou, O. *CrystEngComm* **2013**, *15*, 706−720.
(16) Le Natur, F.; Calvez, G.; Daiguebonne, C.; Guillou, O.; Bernot, K.; Ledoux, J.; Le Polles, L.; Roiland, C. *Inorg. Chem.* **2013**, *52*, 6720−6730.
(17) Lan, A. J.; Li, K. H.; Wu, H. H.; Olson, D. H.; Emge, T. J.; Ki, W.; Hong, M. C.; Li, J. *Angew. Chem., Int. Ed.* **2009**, *48*, 2334−2338.
(18) Feng, J.; Zhang, H. J. *Chem. Soc. Rev.* **2013**, *42*, 387−410.
(19) Cui, Y.; Yue, Y.; Qian, G.; Chen, B. *Chem. Rev.* **2012**, 1126−1162.
(20) Cui, Y.; Xu, H.; Yue, Y.; Guo, Z.; Yu, J.; Chen, Z.; Gao, J.; Yang, Y.; Qian, G.; Chen, B. *J. Am. Chem. Soc.* **2012**, *134*, 3979−3982.
(21) Dang, S.; Zhang, J. H.; Sun, Z. M. *J. Mater. Chem.* **2012**, *22*, 8868−8873.
(22) Dang, S.; Min, X.; Yang, W.; Yi, F. Y.; You, H.; Sun, Z. M. *Chem.—Eur. J.* **2013**, *19*, 17172−17179.
(23) Calvez, G.; Bernot, K.; Guillou, O.; Daiguebonne, C.; Caneschi, A.; Mahé, N. *Inorg. Chim. Acta* **2008**, *361*, 3997−4003.
(24) Bernot, K.; Luzon, J.; Caneschi, A.; Gatteschi, D.; Sessoli, R.; Bogani, L.; Vindigni, A.; Rettori, A.; Pini, M. G. *Phys. Rev. B* **2009**, *79*, 1344191−11.
(25) Jeon, J. R.; Clérac, R. *Dalton Trans.* **2012**, *41*, 9569−9586.
(26) Pearson, R. G. *Coord. Chem. Rev.* **1990**, 403−425.
(27) Pearson, R. G. *J. Am. Chem. Soc.* **1963**, *85*, 3533−3539.
(28) Binnemans, K. *Chem. Rev.* **2009**, *109*, 4283−4374.
(29) Qiu, Y.; Daiguebonne, C.; Liu, J.; Zeng, R.; Kerbellec, N.; Deng, H.; Guillou, O. *Inorg. Chim. Acta* **2007**, *360*, 3265−3271.
(30) Guillou, O.; Daiguebonne, C. Lanthanide ions containing coordination polymers. In *Handbook on the Physics and Chemistry of Rare Eaths;* Gschneider, K. A., Bünzli, J. C. G., Pecharsky, V. K., Eds.; Elsevier: Amsterdam, 2005; Vol. *34*, pp 359−404.
(31) Reneike, T. M.; Eddaoudi, M.; Fehr, M.; Kelley, D.; Yaghi, O. M. *J. Am. Chem. Soc.* **1999**, *121*, 1651−1657.
(32) Daiguebonne, C.; Kerbellec, N.; Guillou, O.; Bünzli, J. C. G.; Gumy, F.; Catala, L.; Mallah, T.; Audebrand, N.; Gérault, Y.; Bernot, K.; Calvez, G. *Inorg. Chem.* **2008**, *47*, 3700−3708.
(33) Daiguebonne, C.; Kerbellec, N.; Gérault, Y.; Guillou, O. *J. Alloys Compd.* **2008**, *451*, 372−376.
(34) Daiguebonne, C.; Kerbellec, N.; Bernot, K.; Gérault, Y.; Deluzet, A.; Guillou, O. *Inorg. Chem.* **2006**, *45*, 5399−5406.
(35) Wang, Z.; Yang, Y.; Cui, Y.; Wang, Z.; Qian, G. *J. Alloys Compd.* **2012**, *510*, L5−L8.
(36) Decadt, R.; Van Hecke, K.; Depla, D.; Leus, K.; Weidenberg, D.; Van Driessche, I.; Van der Voort, P.; Van Deun, R. *Inorg. Chem.* **2012**, *51*, 11623−11634.
(37) Calvez, G.; Daiguebonne, C.; Guillou, O. *Inorg. Chem.* **2011**, *50*, 2851−2858.
(38) Calvez, G.; Le Natur, F.; Guillou, O. Procédé de marquage d'au moins un matériau comprenant une matrice solide ou liquide, organique ou minérale, et matériau correspondant. FR2995316-A1, 2013.
(39) Daiguebonne, C.; Guillou, O.; Kerbellec, N. Procédéde marquage de matériaux à base de matrices organiques polymériques thermoplastiques ou thermodurcissables. FR2917226-A1, 2007.
(40) Daiguebonne, C.; Guillou, O.; Kerbellec, N. Procédé de marquage d'un matériau comprenant au moins une matrice minérale et matériau correspondant. FR2906393-A1, 2006.
(41) Daiguebonne, C.; Gérault, Y.; Guillou, O.; Lecerf, A.; Boubekeur, K.; Batail, P.; Kahn, M.; Kahn, O. *J. Alloys Compd.* **1998**, *275−277*, 50−53.
(42) Groziak, M. *Am. J. Therap.* **2001**, *8*, 321−328.
(43) Hall, D. G. *Boronic Acids;* Wiley-VCH Verlag: Weinheim, Germany, 2005.
(44) Ouchi, K.; Saito, S.; Shibukawa, M. *Inorg. Chem.* **2013**, *52*, 6239−6241.
(45) Regueiro-Figueroa, M.; Djanashvili, K.; Esteban-Gomez, D.; Chauvin, T.; Toth, E.; de Blas, A.; Rodriguez-Blas, T.; Platas-Iglesias, C. *Inorg. Chem.* **2010**, *49*, 4212−4223.
(46) Frullano, L.; Rohovec, J.; Aime, S.; Maschmeyer, T.; Prata, M. I.; Pedroso de Lima, J. J.; Geraldes, C. F. G. C.; Peters, J. A. *Chem.—Eur. J.* **2004**, *10*, 5205−5217.
(47) Allen, F. H. *Acta Crystallogr., Sect. B* **2002**, *B58*, 380−388.
(48) Bruno, I. J.; Cole, J. C.; Edgington, P. R.; Kessler, M.; Macrae, C. F.; Mc Cabe, P.; Pearson, J.; Taylo, R. *Acta Crystallogr., Sect. B* **2002**, *B58*, 389−397.
(49) Lekshmi, N. S.; Pedireddi, V. R. *Inorg. Chem.* **2006**, *45*, 2400−2402.
(50) Desreux, J. F. In *Lanthanide Probes in Life, Chemical and Earth Sciences;* Choppin, G. R., Bünzli, J. C. G., Eds.; Elsevier: Amsterdam, 1989.
(51) Shannon. *Acta Crystallogr., Sect. A* **1976**, *32*, 751.
(52) Daiguebonne, C.; Deluzet, A.; Camara, M.; Boubekeur, K.; Audebrand, N.; Gérault, Y.; Baux, C.; Guillou, O. *Cryst. Growth Des.* **2003**, *3*, 1015−1020.
(53) Henisch, H. K. *Crystals in Gels and Liesegang Rings;* Cambridge University Press: Cambridge, U.K., 1988.
(54) Henisch, H. K.; Rustum, R. *Crystal Growth in Gels;* The Pennsylvania State University Press: University Park, PA, 1970.
(55) Kraus, W.; Nolze, G. *J. Appl. Crystallogr.* **1996**, *29*, 301−303.
(56) Roisnel, T.; Rodriguez-Carjaval, J. *J. Mater. Sci. Forum* **2001**, *378*, 118−123.
(57) Roisnel, T.; Rodriguez-Carjaval, J. In *Materials Science Forum,* Proceedings of the Seventh European Powder Diffraction Conference (EPDIC 7); Scitec: Zurich, Switzerland, 2000; pp 118−123
(58) Le Bail, A. *Powder Diffr.* **2004**, *19*, 249−254.
(59) Shinley, R. *The CRYSFIRE System for Automatic Powder Indexing;* Lattice Press: Surrey, England, 2002.
(60) Altomare, A.; Burla, M. C.; Camalli, M.; Cascarano, G.; Giacovazzo, C.; Guagliardi, A.; Moliterni, A. G. G.; Polidori, G.; Spagna, R. *J. Appl. Crystallogr.* **1999**, *32*, 115−119.
(61) Sheldrick, G. M.; Schneider, T. R. *Methods Enzymol.* **1997**, 319−343.
(62) Farrugia, L. J. *J. Appl. Crystallogr.* **1999**, *32*, 837−838.
(63) Sluis, P.; Spek, A. L. *Acta Crystallogr., Sect. A* **1990**, *A46*, 194−201.

DOI: 10.1021/acs.inorgchem.5b00635
Inorg. Chem. 2015, 54, 5534−5546

(64) Altomare, A.; Burla, M. C.; Camalli, M.; Carrozzini, B.; Cascarano, G.; Giacovazzo, C.; Guagliardi, A.; Moliterni, A. G. G.; Polidori, G.; Rizzi, A. C. *J. Appl. Crystallogr.* **1999**, *32*, 339−340.
(65) Wyszecki, G., Colorimetry. In *Handbook of Optics;* Driscoll, W. G., Vaughan, W., Eds.; MacGraw-Hill Book Company: New York, 1978.
(66) CIE. *International Commission on Illumination - Technical Report;* CIE: 1995; Vol. *13*−*3*.
(67) Casanova, D.; Llunell, M.; Alemany, P.; Alvarez, S. *Chem.—Eur. J.* **2005**, *11*, 1479−1494.
(68) Lekshmi, N. S.; Pedireddi, V. R. *Cryst. Growth Des.* **2007**, *7*, 944−949.
(69) Massiot, D.; Fayon, F.; Capron, M.; King, I.; Le Calvé, S.; Alonso, B.; Durand, J.-O.; Bujoli, B.; Gan, Z.; Hoatson, G. *Magn. Reson. Chem.* **2012**, *40*, 70−76.
(70) Sessoli, R.; Gatteschi, D.; Caneschi, A.; Novak, M. A. *Nature* **1993**, *365*, 141.
(71) Gatteschi, D.; Sessoli, R.; Villain, J. *Molecular Nanomagnets;* Oxford University Press: Oxford, U.K., 2006.
(72) Mannini, M.; Pineider, F.; Sainctavit, P.; Danieli, C.; Otero, E.; Sciancalepore, C.; Talarico, A. M.; Arrio, M. A.; Cornia, A.; Gatteschi, D.; Sessoli, R. *Nat. Mater.* **2009**, *8*, 194−197.
(73) Lehmann, J.; Gaita-Arino, A.; Coronado, E.; Loss, D. *Nat. Nanotech.* **2007**, *2*, 312−317.
(74) Bogani, L.; Wernsdorfer, W. *Nat. Nanotech.* **2008**, *7*, 179−186.
(75) Leuenberger, M. N.; Loss, D. *Nature* **2001**, 789−793.
(76) Rinehart, J. D.; Long, D.-L. *Chem. Sci.* **2011**, *2*, 2078−2085.
(77) Benelli, C.; Gatteschi, D. *Chem. Rev.* **2002**, *102*, 2369−2387.
(78) Woodruf, D. N.; Winpenny, R. E. P.; Layfield, R. A. *Chem. Rev.* **2013**, *113*, 5110−5148.
(79) Cole, K. S.; Cole, R. H. *J. Chem. Phys.* **1941**, *9*, 341−351.
(80) Mydosh, J. A. *Spin Glasses: An Experimental Introduction;* Taylor & Francis: London, U.K., 1993.
(81) Rinehart, J. D.; Long, J. R. *Chem. Sci.* **2011**, *2*, 2078−2085.
(82) Shi, M.; Li, F.; Yi, T.; Zhang, D.; Hu, H.; Huang, C.-H. *Inorg. Chem.* **2005**, *44*, 8929.
(83) Prodi, L.; Maestri, M.; Ziessel, R.; Balzani, V. *Inorg. Chem.* **1991**, *30*, 3798−3802.
(84) Quici, S.; Cavazzini, M.; Marzanni, G.; Accors, i. G.; Armaroli, N.; Ventura, B.; Barigelletti, F. *Inorg. Chem.* **2005**, *44*, 529−537.
(85) Bünzli, J. C. G.; Eliseeva, S. V. Basics of Lanthanide Photophysics. In *Lanthanide Luminescence;* Hänninen, P., Härmä, H., Eds. Springer: Berlin Heidelberg, 2010.
(86) Steemers, F. J.; Verboom, W.; Reinhoudt, D. N.; Van der Tol, E. B.; Verhoeven, J. W. *J. Am. Chem. Soc.* **1995**, *117*, 9408−9414.
(87) Eliseeva, S. V.; Bünzli, J. C. G. *Chem. Soc. Rev.* **2010**, *39*, 189−227.
(88) Latva, M.; Takalo, H.; Mukkala, V.-M.; Matachescu, C.; Rodriguez-Ubis, J. C.; Kankare, J. *J. Lumin.* **1997**, *75*, 149−169.
(89) D'Aléo, A.; Pointillart, F.; Ouahab, L.; Andraud, C.; Maury, O. *Coord. Chem. Rev.* **2012**, *256*, 1604−1620.
(90) Comby, S.; Bünzli, J. C. G.; Gschneider, K. A.; Pecharsky, V. K. Lanthanide Near-Infrared Luminescence in Molecular Probes and Devices. In *Handook on the Physics and Chemistry of Rare Earths;* Elsevier: Amsterdam, 2007; Vol. *37*.
(91) Werts, M. H. V.; Jukes, R. T. F.; Verhoeven, J. W. *Phys. Chem. Chem. Phys.* **2002**, *4*, 1542−1548.
(92) Arakcheeva, A.; Logvinovich, D.; Chapuis, G.; Morozov, V.; Eliseeva, S. V.; Bünzli, J. C. G.; Pattison, P. *Chem. Sci.* **2012**, *3*, 384−390.
(93) Carnall, W. T.; Fields, P. R.; Rajnak, K. *J. Chem. Phys.* **1968**, *49*, 4450−4455.
(94) Carnall, W. T.; Fields, P. R.; Rajnak, K. *J. Chem. Phys.* **1968**, *49*, 4447−4450.
(95) Wertz, M. H. V.; Jukes, R. T. F.; Verhoeven, J. W. *Phys. Chem. Chem. Phys.* **2002**, *4*, 1542−1548.
(96) Haquin, V.; Etienne, M.; Daiguebonne, C.; Freslon, S.; Calvez, G.; Bernot, K.; Le Polles, L.; Ashbrook, S. E.; Mitchell, M. R.; Bünzli, J. C. G.; Guillou, O. *Eur. J. Inorg. Chem.* **2013**, 3464−3476.
(97) Bünzli, J.-C. G.; Comby, S.; Chauvin, A.-S.; Vandevyver, C. D. B. *J. Rare Earths* **2007**, *25*, 257−274.
(98) Cui, Y.; Xu, H.; Yue, Y.; Guo, Z.; Yu, J.; Chen, Z.; Gao, J.; Yang, Y.; Qian, G.; Chen, B. *J. Am. Chem. Soc.* **2012**, *134*, 3979−3982.
(99) Rao, X.; Song, T.; Gao, J.; Cui, Y.; Yang, Y.; Wu, C.; Chen, B.; Qian, G. *J. Am. Chem. Soc.* **2013**, *135*, 15559−15564.

DOI: 10.1021/acs.inorgchem.5b00635
Inorg. Chem. 2015, 54, 5534−5546